Journal of Environmental Chemical Engineering 11 (2023) 111523

Contents lists available at ScienceDirect

Journal of Environmental Chemical Engineering

journal homepage: www.elsevier.com/locate/jece

How to guide photocatalytic applications of titanium dioxide co-doped with nitrogen and carbon by modulating the production of reactive oxygen species

Alessia Zollo [a], Stefano Livraghi [a,*], Elio Giamello [a], Andrea Cioni [b], Valentina Dami [b], Giada Lorenzi [b], Giovanni Baldi [b], Stefano Agnoli [c], Mateusz Adam Baluk [d], Anna Gołąbiewska [d], Adriana Zaleska-Medynska [d]

[a] Dipartimento di Chimica and NIS, Università di Torino, Via P. Giuria 7, 10125 Torino, Italy
[b] COLOROBBIA CONSULTING S.r.L., Via Pietramarina 53, Sovigliana, Vinci, FL 50053, Italy
[c] Department of Chemical Sciences and INSTM Unit, University of Padova, Via F. Marzolo 1, 35131 Padova, Italy
[d] Department of Environmental Technology, Faculty of Chemistry, University of Gdansk, 80–308 Gdansk, Poland

ARTICLE INFO

Editor: Stefanos Giannakis

Keywords:
Photocatalysis
Visible light
Singlet oxygen
C/N-TiO_2
Carbon moieties

ABSTRACT

A carbon and nitrogen TiO_2 (C/N-TiO_2) photocatalyst has been obtained modifying a commercial TiO_2 using ammonium citrate. The photocatalyst has been tested in two photocatalytic tests under visible light, NOx abatement in gas phase and phenol degradation in liquid phase monitoring in parallel the formation of reactive oxygen species (ROS) via EPR. We achieved a deep insight about its activity, which relies on superoxide and singlet oxygen ($O_2^{-\bullet}$ and $^1O_2$) with no role of $OH^\bullet$ radicals. The singlet oxygen ($^1O_2$) is exclusively a result of the excitation of the surface carbonaceous species and it is essential to oxidize phenol but limits the abatement of nitric oxide. The photocatalyst activity can be modulated according to its actual application tuning the carbon content. The oxidation of phenol in liquid environment is favoured by the presence of the carbonaceous phase while NO abatement is favoured by its partial removal.

1. Introduction

Heterogeneous photocatalysis represents, since the latest decades of the past century, a powerful tool in the areas of solar fuels production [1], pollutant abatement [2–4] and antimicrobial activity [5–7]. Since the discovery of the photocatalytic properties of titanium dioxide (or titania) [8], researchers were attracted by the peculiar properties of this material in photocatalytic reactions related to energy production and environmental applications. Due to a band gap value ranging between 3.0 and 3.2 eV of the most common polymorphs, this oxide can be excited by photons of the UV domain. Photoexcitation of valence band electrons generates two charge carriers (an electron in conduction band and an electron-hole in the valence band) that can either recombine or migrate in the crystal reaching the surface where both are highly reactive entities. The same process in principle occurs for various semiconducting materials having band structure similar to titania, although few other systems have shown the photocatalytic ability of this oxide. This different ability depends on a variety of factors including the charge carrier's mobility, their surface stabilisation, the electron transfer ability and, last but not least, on particularly favourable surface chemistry properties. For various decades the applications of photocatalysis in environmental chemistry were based therefore on the extended use of titania, a relatively cheap and non-toxic material, coupled to UV light sources and mainly in liquid phase (water pollution remediation). In parallel, however, an intense activity has grown, aimed to prepare Visible Light Active (hereafter VLA) photocatalytic systems in order to exploit in a more extensive way the solar radiation in which ultraviolet light is a minor component. The problem is not so trivial as it could, at a first sight, appear since the use of an oxide with band gap compatible with the energy of visible photons involves the consequent variation of the electrochemical potential of the photoexcited carriers with decline of their reactivity.

Various approaches have been followed along the years [9,10] including: i) the use of small band-gap semiconductors such as

* Corresponding author.
E-mail address: stefano.livraghi@unito.it (S. Livraghi).

https://doi.org/10.1016/j.jece.2023.111523
Received 23 August 2023; Received in revised form 27 October 2023; Accepted 15 November 2023
Available online 19 November 2023

oxonitrides or graphitic carbon nitride [11], ii) dispersing metal nanoparticles with plasmonic effect on the solid [12], iii) synthetizing coupled semiconductors with solid-solid heterojunctions reproducing the Z scheme of natural photosynthesis [13] and, iv) engineering the electronic properties of an oxide by doping, *e.g.* by the insertion of a foreign atom into the lattice, with formation of novel states inside the band gap. A breakthrough in this latter field is considered the discovery of nitrogen doped titania (N-TiO_2) at the beginning of the century [14–16]. The efficiency of the various systems based on non-metal modified titania is inconstant and, in short, it can be stated that the performance of a typical TiO_2 photocatalyst (namely the classic Evonik P25, a benchmark system in this field) working under UV illumination in liquid environment is never surpassed, in terms of efficiency, by the new systems. However, the search for VLA photocatalytic systems and for their possible applications continued to be pursued in the first two decades of the century despite the relatively unsatisfactory performances initially monitored for these systems.

The impulse to prepare new and more efficient VLA photocatalytic systems was brought about not only by the mentioned need of employing sunlight in liquid phase photocatalytic processes, for instance for the purification of civil or industrial wastewater, but also by the rising necessity to create efficient devices for the purification of indoor air [17,18], possibly avoiding the use of UV light [19]. Several methodologies can be followed to contrast in-door pollution [20] among which photocatalysis is assuming a growing importance [5].

The success of the photocatalytic approach to face the problem of indoor air quality has been driven by a couple of key factors. The first one is the progressive consolidation of low cost VLA photocatalytic systems active in gas phase reactions and stable over time. The use of ultraviolet, which, by the way, is an energy-intensive light source, is in fact not recommended in indoor environments for the risk of direct exposition and for the tendency to produce ozone and radicals in the atmosphere. The second factor is the advent and diffusion of LED-type lighting that are energy saving sources and emit light at controlled frequency. The matching of adequately performing VLA photocatalysts and LED illumination systems is the base of commercial devices used for indoor air purification and disinfection.

Among the possible VLA photocatalysts, the research on titanium dioxide modified with carbon or nitrogen compounds has been actively pursued in the past [21–25]. As demonstrated by detailed investigations based on Electron Paramagnetic Spectroscopy (EPR) [26–28] N doped TiO_2, due to the introduction of nitrogen atoms in the lattice of the oxide (see below) benefits from peculiar intra band gap states. Concerning the role of carbon, the role in the visible light activity is less straightforward due to the different forms of carbon that can be involved ranging from lattice doping [29] to heterojunctions with structures of different complexity as graphene-based compounds [30,31], C_3N_4 [32,33], carbonaceous species [34,35] including carbon dots [36,37]. Moreover, in some cases also a detrimental effect on the photochemical properties of TiO_2 is also reported [38–40].

Inspired by a commercial nitrogen-modified TiO_2 powder (PHOS000033, WO 2019/211787), in a previous paper from our labs [41], we showed how, starting from a polyphasic titanium dioxide matrix, nitrogen-doped catalysts can be obtained having variable performances related to the compound used to dope the oxide. In particular, if an organic ammonium salt is used, e.g. dibasic ammonium citrate ($C_6H_8O_7{\cdot}2NH_3$), a particularly active photocatalyst is obtained, characterised by the presence, beside bulk nitrogen doping centers, of carbonaceous phases in significant amount. The present paper is devoted to a thorough characterisation of this co-doped material. We aim to describe its structural features, to clarify the role of both modifiers and the mechanism of the photocatalytic processes occurring at its surface. Nitric oxide abatement in gas phase and phenol degradation in liquid phase (performed under illumination with artificial visible light) have been selected to evaluate the photocatalytic activity of the system.

2. Experimental

2.1. Material

The VLA photocatalyst was obtained by the modification of a commercial TiO_2 suspension (PARNASOS® PH000025, COLOROBBIA CONSULTING S.r.l., Vinci, Italia) via modification with dibasic ammonium citrate ($C_6H_8O_7{\cdot}2NH_3$) according to a procedure proposed in a previous work of some of the authors [42]. An appropriate amount of the modifier to get a nominal N/Ti molar ratio = 0.035 was employed. The ammonium citrate was mixed with the commercial suspension and the resulting mixture was then recovered via spray-dry procedure. The so obtained mix of powders was then calcined at 743 K for 60 min using a heating rate of 6.2 K/min. Hereafter, the prepared photocatalyst will be labelled as C/N-TiO_2.

2.2. Material characterisation

2.2.1. BET surface area

The specific surface area was measured with a Micromeritics ASAP 2020 apparatus using the Brunauer–Emmett–Teller (BET) model for N_2 adsorption measurements. Prior to N_2 adsorption, the sample was outgassed at 573 K for 2 h.

2.2.2. X-Ray Diffraction (XRD)

Powder X-ray diffraction (XRD) patterns were recorded with a PANalytical PW3040/60 X'Pert PRO MPD diffractometer using a copper Kα radiation source and the X'Pert High-Score software was used for data handling. Diffraction patterns were refined with Rietveld method using MAUD (Material Analysis Using Diffraction) program.

2.2.3. Diffuse Reflectance Spectroscopy (DRS)

The UV-Visible Diffuse Reflectance (DR-UV-Vis) spectra were recorded using a Varian Cary 5000 spectrometer. A Polytetrafluoroethylene (PTFE) sample was used as the reference. The spectrum was recorded in the 200–800 nm range at a scan rate of 240 nm/min with a step size of 1 nm. The measured reflectance was converted with the Kubelka-Munk function and the Tauc plot method was employed to evaluate the Band Gap energy.

2.2.4. Thermogravimetric analysis coupled with gas phase FTIR (TGA-FTIR)

TGA was performed using an ultra-microbalance (sensitivity: 0.1 mg) coupled with FTIR detector for the analysis of the evolved volatiles. A heating ramp from 308 K to 1073 K (rate: 20 K/min^{-1}) in presence of oxygen (flow rate: 35 mL•min^{-1}) in a Pyris 1 TGA (Perkin-Elmer, Waltham, USA). Evolved species were continuously analyzed in the 4000–600 cm^{-1} wavenumber range (resolution: 0.4 cm^{-1}) by the FTIR detector (Perkin-Elmer, Spectrum 100) with a thermo-stated conventional gas cell. FTIR profiles of volatiles (mainly water and carbon dioxide) were obtained following the intensity of peaks at 1650 cm^{-1} (water O-H bending), and 2353 cm^{-1} (CO_2 asymmetric stretch).

2.2.5. Solid state continuous wave EPR (CW-EPR)

Solid state EPR spectra were acquired using a Bruker EMX spectrometer operating at X-band (9.5 GHz), equipped with a cylindrical cavity operating at 100 kHz field modulation. All the spectra were recorded at room temperature (RT) with a 1 mW of incident microwave power and with a modulation amplitude of 0.2 mT.

2.2.6. Spin trapping experiments

Two different spin trapping molecules were used: 5,5-Dimethyl-1-pyrroline N-oxide (DMPO, Sigma Aldrich) was employed for hydroxyl radical, superoxide and, together with formate, for holes detection while 2,2,6,6-Tetramethyl-4-piperidone (TEMP-H, Sigma-Aldrich) for singlet oxygen detection. EPR spectra were recorded at room temperature using

a X-band benchtop EPR spectrometer (ADANI's SPINSCAN X). Ex situ irradiation experiments to monitor the formation of the radicals were performed using a blue LED (λ = 460 nm) and a fan in order to avoid sample heating. The samples were prepared suspending 10 mg of photocatalyst in i) 0.5 mL of DMPO aqueous solution 0.044 M for the hydroxyl radical; ii) 0.5 mL of aqueous solution buffered at basic pH containing DMPO 0.044 M and sodium formate (0.5 M) for holes detection; iii) 0.5 mL of DMPO solution (0.044 M) in acetonitrile instead of water to avoid competition with hydroxyl radicals for the superoxide species; iv) 0.5 mL of 4-oxo-TEMP-H aqueous solution (0.044 M) buffered at basic pH for singlet oxygen detection.

2.2.7. X-ray photoelectron spectroscopic (XPS) analysis

XPS analysis was performed to examine the composition of the samples. The Binding Energies (BE) were calibrated internally setting the position of the peak of adventitious carbon in the C 1s spectrum at an energy of 284.6 eV.

2.3. Photocatalytic tests

2.3.1. NO abatement test

Capability in NO abatement has been tested under two different irradiation conditions, i) upon blue light illumination obtained using a blue LED (465 nm) source with an incident irradiance of 58 W/m^2 (detection range 400–800 nm), ii) upon white light illumination obtained using a white (3000 K) LED source with an incident irradiance of 87 W/m^2 (detection range 400–800 nm). For the test, a powder suspension (5% w/w in water) was used to coat via spray-gun glass substrate (100 mm ± 0.10 ×100 ± 0.10 mm) and approximately 0.15 g of dry product was employed in each test.

The analyses were performed using a discontinuous mode where the reaction chamber is connected to a bag and to a peristaltic pump, in order to create a closed circuit. The bag works as reservoir from which it is possible to send the pollutant atmosphere to the measuring instrument. The test consists of six samplings of 5 min each, alternated with 15 min of recirculation, for a total time of analysis of 105 min.

The dry air, moist air and nitric oxide were mixed in proportions such as to obtain a fixed nitric oxide concentration of around 500 ± 50 ppbv in an atmosphere having about 50 ± 10% of relative humidity at a temperature of about 298 ± 5 K.

2.3.2. Photocatalytic phenol abatement test

The phenol degradation test in liquid phase was carried out using a well-established protocol for the evaluation of the activity of photocatalysts. Briefly, in the reactor 0.125 g of the sample in 25 mL of aqueous phenol solution (20 mg/L). The visible light irradiation (λ > 420 nm) was performed with a 1000 W Xenon lamp. To establish the absorption–desorption equilibrium, the reactor was kept without light for 30 min. The suspension was then irradiated for 60 min with continuous magnetic stirring and air bubbling (5 dm^3/h) at the constant temperature of 283 ± 0.5 K. Every 20 min, 0.5 mL of the suspension were collected and filtered through a 0.2 μm syringe filter. Phenol degradation was followed with high performance liquid chromatography (HPLC, Shimadzu) equipped with a Kinetex C18 column (150 × 3 mm, particle size 2.6 μm, pore diameter 100 Å) and SPD-M20A diode array detector operated at 275 nm for phenol and 225 nm for major degradation intermediates (p-benzoquinone, hydroquinone and catechol). The mobile phase was composed of acetonitrile and trifluoroacetic acid (10/90, v/v) with a constant flow rate of 0.55 mL/min.

3. Results and discussion

3.1. Phase composition and optical absorption

The XRD characterization of the photocatalyst indicates that the material has a polyphasic composition and that it is made up by the three main polymorphs of titanium dioxide, namely anatase, rutile and brookite in different percentages (Fig. 1A and Table 1) and with different crystallite size as pointed out in Table 1 (data extrapolated from the XRD patterns and TEM analysis, see Supporting Information). It is worth recalling that the starting bare TiO_2 is also a triphasic material even though the fraction of the different polymorphs changes along the thermal treatment of modification [33,42].

The optical absorption between 350 nm and 1200 nm of the materials is reported in Fig. 1B. In the spectrum it is possible to identify two absorption regions, the typical valence band to conduction band transition in the UV, and a second weaker absorption spread all over the visible region until the near infra-red (NIR), whose magnification is reported in panel B′ in Fig. 1. It is worth to mention that for titania doped exclusively with nitrogen (N-TiO_2) the expected absorption in the visible region is usually confined in a well-defined region in the range 400–500 nm (See Fig S.I. 2) [43]. The extension of the optical absorption until the NIR suggests that carbon containing residues are also present. The Tauc's plot method indicates a nominal absorption threshold value of about 3.0 eV (Panel B" in Fig. 1) due to the high content of the rutile polymorph.

3.2. Carbonaceous species at the TiO_2 surface

Since the optical absorption indicates that carbonaceous species are likely present in this material, TGA-FTIR and XPS analysis have been performed in order to characterize this component of the solid. The weight loss of the sample upon heating under oxygen atmosphere was monitored in the temperature range between 308 K and 900 K and it is reported in Fig. 2, red line. The total weight loss of the material is about 1.6% w/w. In the thermogram, three main events have been recorded, as shown by the derivative curve in Fig. 2, panel A, blue line. The first one, at around 353 K, is due to a loss of physisorbed water from the surface of the system as indicated by the low temperature value and by the water FTIR profile in panel B. This first desorption event account for about 30% of the total weight loss. The second thermogravimetric event occurs at 473 K. At this temperature, together with water, carbon dioxide release is observed in the gas phase FTIR spectrum (Fig. 2, panel B). This temperature is too low to be explained in terms of oxidation of organic residues, hence we can ascribe this event to the loss of chemisorbed water molecules accompanied by the decomposition of carbonate-like species whose presence is also confirmed by the IR analysis (see S.I.). Finally, the last weight loss event is registered at about 623 K, due to carbon residues combustion. No evidence of the evolution of nitrogen containing species was observed suggesting that the content of nitrogen is below the detection limit of the instrument.

X-ray Photoelectron Spectroscopy (XPS) was employed to assess the surface elemental composition of the material (see S.I.). The XPS analysis indicates the presence of a relatively abundant surface carbonaceous phase much higher of the total nitrogen content (atomic composition: Ti = 22.2%, C = 17.8%, O = 59.3% N = 0.7%). As far as the nitrogen is concerned, XPS signal is centred at about 400 eV indicating the presence of interstitial nitrogen which is reported to be associated to isolated intra band gap energy states from which it is possible to promote electrons in conduction band by the solely visible light.[26] It is worth to mention however that the binding energy of about 400 eV can be due to nitrogen byproducts also.[44] Nevertheless, the presence of dopant nitrogen is definitely confirmed by the solid state EPR characterization (see Section 3.3 and S.I.). As far as the carbon component, the C 1s photoemission spectrum in Fig. 3 comprises a main peak at 284.8 eV, distinctive of adventitious or C sp^3, and another intense component typical of C sp^2 at 284.4 eV. Moreover, some peaks associated with oxidized species can be observed at 286.5 eV and 289.0 eV; whereas it is not possible to observe any chemically shifted component related to carbon species inside the titania lattice that are normally observed below 283.5 eV. Overall, the XPS data suggest the presence of carbon species formed during the last calcination step that

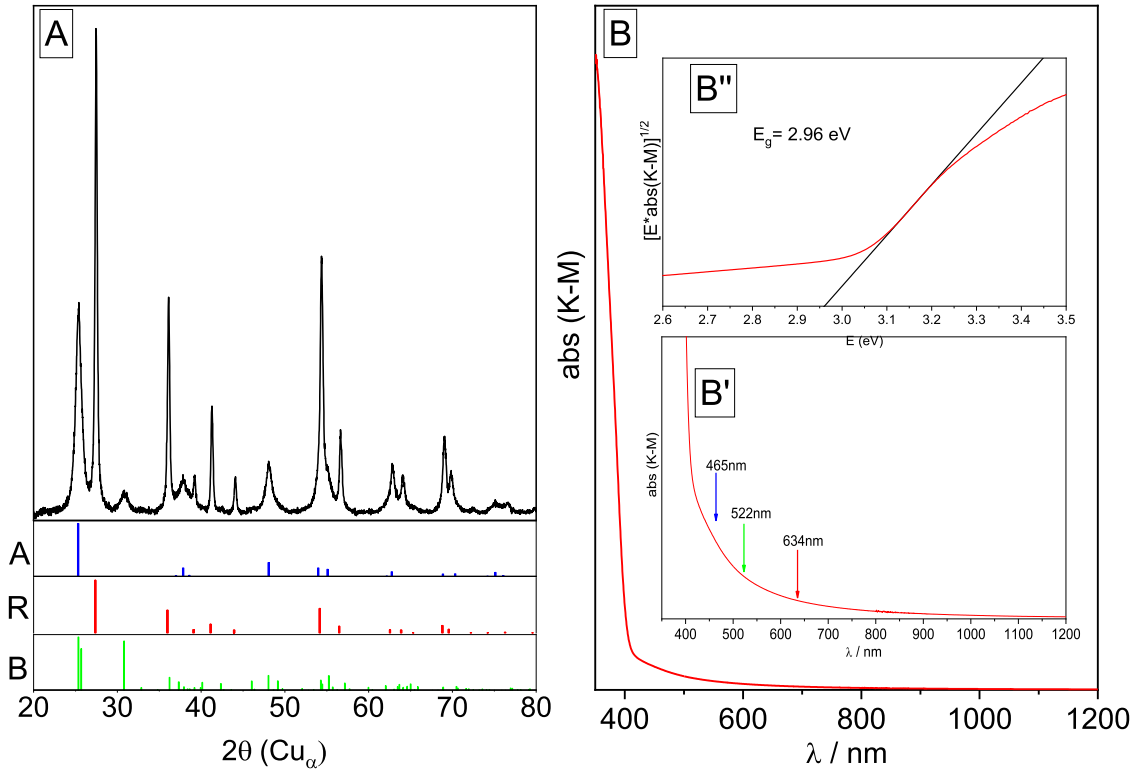

Fig. 1. Panel A: X-Ray diffraction pattern (XRD) of the C/N-TiO_2 sample.In the lower part of the panel the expected diffraction peaks for the three TiO_2 polymorphs (A= anatase, R= rutile, B= brookite). Panel B: DR-UV-Vis-NIR spectrum of the material. Inset B' shows the magnification of the absorption in the visible light range. Inset B'' shows the Tauc's plot and the corresponding extrapolated band gap threshold.

Table 1
Phase composition, surface area, crystal size and band gap energy value of the C/N-TiO_2 photocatalyst.

Material	Specific surface area (m^2/g)	Band gap value E_g (eV)	Anatase fraction /% (*Crystal size*/nm)	Rutile fraction /% (*Crystal size*/nm)	Brookite fraction /% (*Crystal size* /nm)
C/N-TiO_2	66	3.0	33 – (*15*)	53 – (*47*)	14 – (*14*)

are somehow reminding of the so called carbon dots, which are characterized by a C sp^2/C sp^3 core and connected to the oxide through carboxylate or alcoholate bonds.

As far as the carbonaceous fraction is concerned, recently Carbon Quantum Dots (CQDs) have attracted the attention of researchers mainly for their optical properties (e.g. strong fluorescence) allowing several important applications in biosensing and nanomedicine[45] but also, because of their optical absorption in a wide range of visible wavelengths, in photocatalysis. It is also interesting, to the scopes of the present paper, to notice that the same compound here used to dope titania (ammonium citrate) is also used, in some cases, for the preparation of nitrogen doped CQDs[46] that are carbon rich and have a potential use in different research field. CQDs are non-stoichiometric compounds with variable compositions. There is often a carbon core that may be either amorphous or crystalline containing, in this latter case, graphitic carbon or graphene and graphene oxide. The external surface can be oxidized at different extents till a relevant amount of oxygen content. The presence on C/N-TiO_2 of a surface phase with properties somehow similar to those of CQDs is corroborated by the fluorescence spectra that show a strong fluorescent emission with a maximum varying between 590 nm and 570 nm according to the wavelength of the exciting radiation (See S.I.). The evident analogies between the behaviour of the carbonaceous phase on C/N-TiO_2 and that of CQDs does not mean that this phase, formed by interaction of ammonium citrate on the titanium dioxide support, contains true CQDs. The synthesis of CQDs, in fact, must follow well-defined protocols that involve temperatures lower than that used in our case for the final calcination treatment of C/N-TiO_2. Furthermore, in the case of CQD/TiO_2 hybrids reported in the literature, the carbon quantum dots are preliminarily prepared and then deposited on the solid by a treatment in mild conditions[47].

3.3. EPR characterization

The presence of an optical absorption in the visible does not automatically imply the existence of photoactivity in the same range of frequency. Photoactivity occurs when incident photons produce an excitation in the solid systems with generation of reactive charge carriers. One of the most suitable tools for their detection is the Electron Paramagnetic Resonance (EPR) technique that has progressively assumed a prominent role in the characterisation of photocatalytic systems and related phenomena [48]. We have therefore monitored by EPR the effect of irradiation in various conditions both at the gas-solid and liquid-solid interfaces [49,50].

3.3.1. Solid state EPR characterization at room temperature (RT)

To understand the effect of irradiation on the photocatalyst it is necessary, first, to describe the corresponding EPR spectrum recorded in the dark, as paramagnetic centres are already present in the starting material. This is reported in Fig. 4, Panel A (black line) and is due to two distinct, highly overlapped, signals. The first one, dominating the spectrum, is a symmetric unstructured Lorentzian line centred at g = 2.003 which is typical of carbonaceous materials. The corresponding paramagnetic species will be hereafter labelled as $C^{\bullet}$. The computer simulation of the experimental spectrum indicates that the abundance of

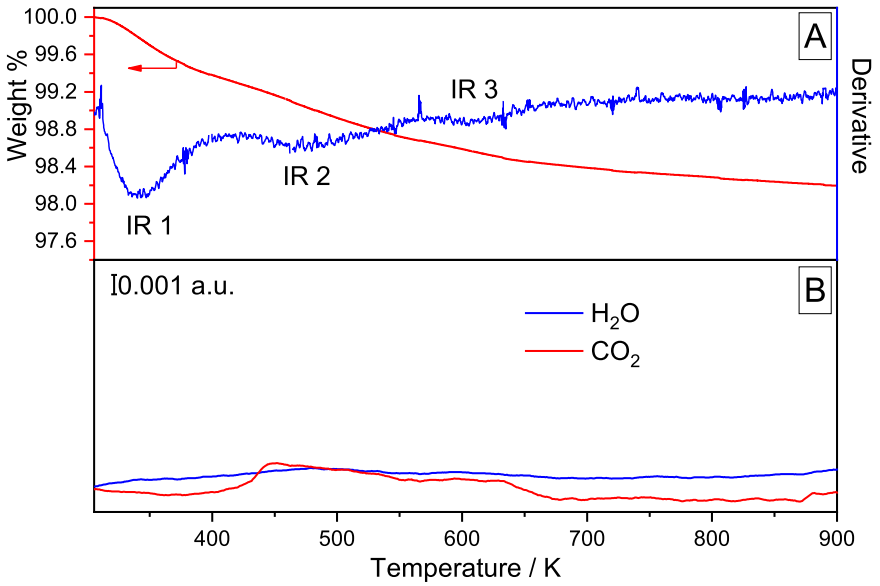

Fig. 2. TGA-FTIR profile for the C/N-TiO_2 material. Panel A: weight loss (red line) and related first derivative (blue line). Panel B: IR-detected profile related to water and carbon dioxide emission.

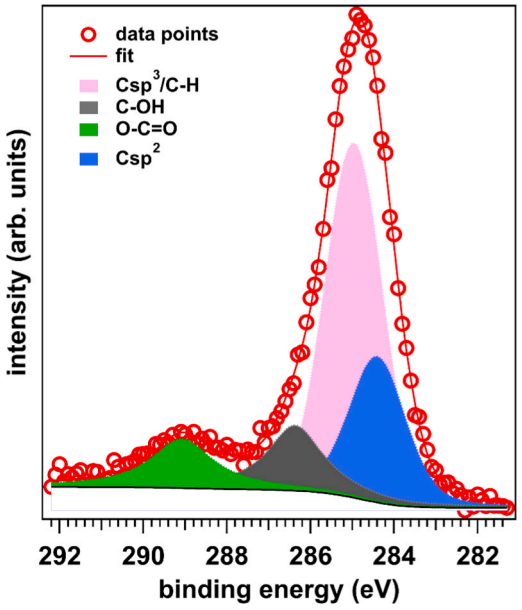

Fig. 3. C 1 s XPS spectrum of C/N-TiO_2.

this species accounts for about 90% of the total intensity (See Supporting Information).

The second signal is a minority component (10%) of the whole spectrum and it is based on a central line surrounded by two external wings. The signal is due to a well-known paramagnetic species reported by some of us in the past, widely investigated along the years [36] and that can be considered a fingerprint of the effective insertion of N in the titania bulk. The two weak wings are part of a hyperfine triplet due to N (interaction of the unpaired electron with a single ^{14}N nucleus having nuclear spin I=1, hence multiplicity = 2I+1 = 3). The signal corresponds to a N containing species in the bulk of titania formally written as $NO^{2-\bullet}$ (the actual charge is likely lower) and that can be described as a N atom bound to a O^{2-} ion of the titania lattice. Beside this species, a corresponding diamagnetic one, NO^{3-}, is always present in the lattice. The joint use of experimental and theoretical investigations has shown that intra band gap energy states are associated to these two species (NO^{2-} and NO^{3-}) which are responsible for the visible light sensitization of TiO_2 [26].

$NO^{2-\bullet}$ is the only paramagnetic species observed in EPR spectra obtained in case of N-TiO_2 materials produced using ammonia or ammonium inorganic salts as nitrogen source: in those cases, its behaviour can be more easily studied in the absence of the intense signal due to carbonaceous species. Nonetheless data in Fig. 4 confirm that, as in the case of the solely N-doped TiO_2 system, the intensity of the species grows under irradiation in vacuum condition, in a minor extent with green light ($\lambda = 522$ nm) and more significantly with blue light ($\lambda = 465$ nm), due to the photoexcitation of an electron from the diamagnetic, and more abundant, NO^{3-} species as described by Eq. 1. As reported in previous papers, the visible light is able to promote electrons from nitrogen-related intra band gap states to the TiO_2 conduction band (C.B.), and due to the absence of electron scavengers, the process is reversible [27].

$$NO^{3-}(\uparrow\downarrow) + h\nu \leftrightarrows NO^{2-\bullet}(\uparrow) + e^{-}(C{\cdot}B{\cdot}) \quad (1)$$

$$e^{-}(C{\cdot}B{\cdot}) + Ti^{4+} \leftrightarrows Ti^{3+} \quad (2)$$

This is further proved by the spectra related to the same experiment but recorded at low temperature (77 K) show, additionally, the formation of Ti^{3+} ions (undetectable at RT) due to the stabilisation of the photoexcited electrons by the surface of the oxide (Eq. 2, see S.I.). Notably, the same experiment of irradiation with visible light performed in the presence of air using, in distinct tests, red (634 nm), green (522 nm) and blue LED (465 nm) lights respectively (Fig. 4B) have the same effect, though at different extent, which is observed in the EPR spectrum (Fig. 4B and magnification) in terms of the appearance of a signal with $g_1 = g_{zz} = 2.025$, $g_2 = g_{yy} = 2.009$ (and with the third component buried in the main line due to $C^{\bullet}$) easily assigned to superoxide ions adsorbed on top of Ti^{4+} ions [51]. The formation of the surface adsorbed superoxide is due to the photoinduced electron transfer from the solid to gaseous oxygen as described by Eq. 3.

$$O_{2\,(gas)} + e^{-}(C{\cdot}B{\cdot}) \rightarrow O_{2\,(ads)}^{-\bullet} \quad (3)$$

As better shown by the magnifications A′ and B′ in Fig. 4, the effect of irradiation in both cases increases lowering the wavelength and it is maximum for blue light. This experiment is particularly important since it demonstrates that photoexcited electrons are reactive, i.e. they reach the surface and reduce molecular oxygen to superoxide, a well-known radical ion belonging to the class of reactive oxygen species (ROS).

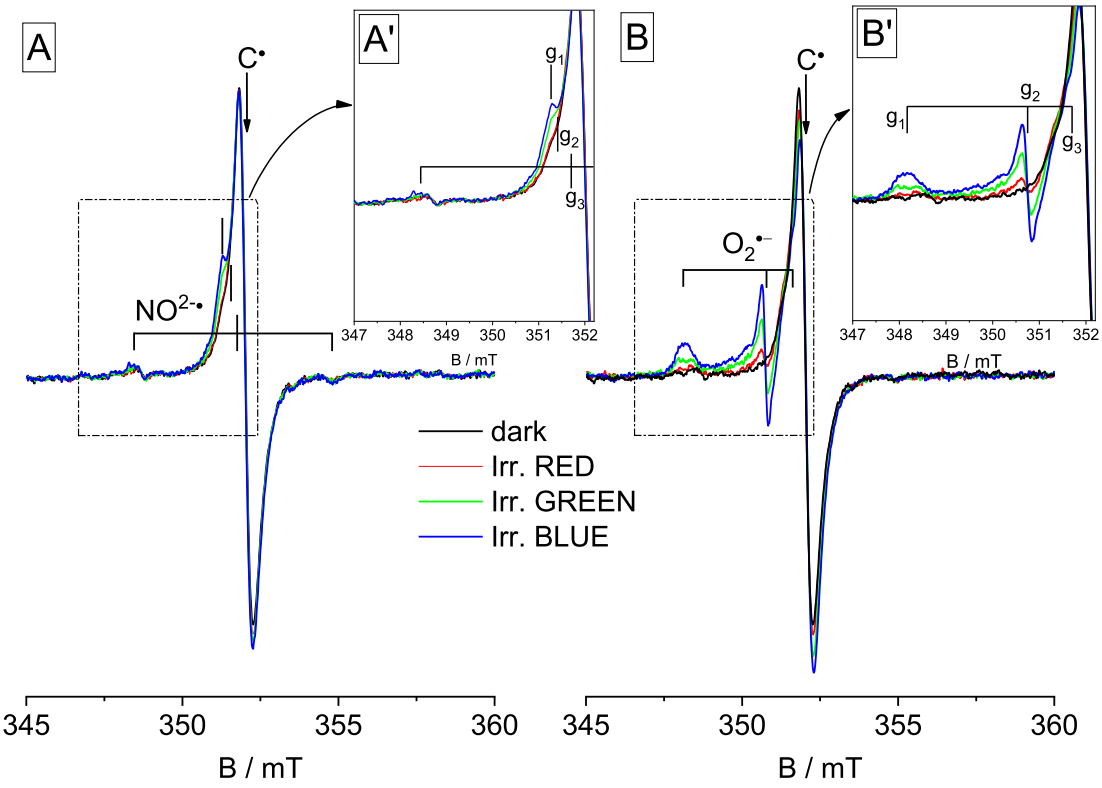

Fig. 4. EPR spectra at RT. Panel A. Spectra of the material recorded in dark and upon illumination with various wavelengths at room temperature and in vacuum conditions. The stick diagram indicates the main features of the $NO^{2-\bullet}$ species. Panel B. EPR spectra recorded in air at room temperature upon illumination with three different LED emitted lights, (red) at 634 nm, (green) at 522 nm and (blue) at 465 nm. Insets A′ and B′ show the region magnification corresponding to the $NO^{2-\bullet}$ species and adsorbed superoxide respectively.

Moreover, this phenomenon, quite common for pristine titania using UV photons, occurs for the photocatalyst here reported using visible light photons in a range of energy spanning from 2.67 eV (blue) to 1.95 eV (red) though at different extent for the various frequencies. We are therefore in the presence of a VLA system whose activity covers a wide portion of visible light. This is not the case of the "classic" nitrogen doped TiO_2 (non-containing carbon) which is active in a narrower window of visible frequencies centred around 270 nm (blue)[24]. This evidence thus suggests that, in the present case, the observed photoactivity is due to the simultaneous presence of nitrogen and carbon modifications.

3.3.2. *Reactive oxygen species (ROS) at the solid-liquid interface*

The generation of reactive oxygen species in solution, under irradiation with visible light, was evaluated via spin trapping experiments (Fig. 6). Two different tests were carried out, first, to monitor the occurrence of charge transfer phenomena involving holes, both using the trapping molecule DMPO in water solution. In the first case the DMPO molecule is able to detect $OH^\bullet$ radicals (formed by interaction of photogenerated holes (h^+) with water or with surface OH^- groups, Eq. 4) forming the stable paramagnetic DMPO-OH adduct. In a similar way, in solutions containing sodium formate, the holes (h^+) react with formate ions producing the $COO^{\bullet-}$ radical ion (Eq. 5) which is easily trapped by DMPO with formation of the paramagnetic DMPO-COO^- adduct.

$$OH^- + h^+ \rightarrow OH^\bullet \quad (4)$$

$$HCOO^- + h^+ \rightarrow COO^{\bullet-} + H^+ \quad (5)$$

The two adducts have distinct EPR spectra so that coupling the two described spin trapping tests one can monitor the presence of photogenerated oxidizing entities (h^+, $OH^\bullet$).

Surprisingly, neither $OH^\bullet$ nor $COO^{\bullet-}$ radicals were detected in the two distinct tests suggesting that in the material under investigation the photocatalytic pathway does not involve photogenerated holes.

We turned thus our attention on the role of photoformed electrons. As reported before (Fig. 4B) the formation of excited electrons under irradiation and their capability of reducing molecular oxygen was observed at the gas-solid interface. To assess the formation of superoxide species also in solution we used the trapping molecule DMPO in acetonitrile to monitor the formation, if any, of the paramagnetic DMPO-O_2^- adduct. Differently from the previous cases, the formation of this adduct was easily detected (Fig. 6). Finally, the formation of singlet oxygen ($^1O_2$) was taken into consideration monitoring its possible presence with a specific trap molecule, the 4-oxo-TEMP-H. In this case the singlet oxygen molecule reacts with the trap generating the paramagnetic 4-oxo-TEMPO species. As shown in Fig. 6, also in this case, clear evidence of the 4-oxo-TEMPO adduct was observed indicating that the $^1O_2$ species is generated under visible light irradiation. Summarizing, the photocatalytic activity in solution of the modified titania is based on the action of two oxidant species ($O_2^{\bullet-}$ and $^1O_2$) formed upon irradiation with visible light while processes based on holes and hole-transfer seems to be absent.

3.4. *Photocatalytic tests*

3.4.1. *Photocatalytic activity under visible light in gas phase*

The C/N-TiO_2 material described in this paper has been tested in the photocatalytic reaction of nitric oxide (NO) abatement under two distinct types of LED-generated visible light, monochromatic blue and white (3000 K) respectively, in the absence of any UV component. The test was performed in a gas phase simulating the atmosphere composition (O_2, N_2 and H_2O). In the test we have monitored the concentration

of both NO and NO_2 as a function of irradiation time (Fig. 7). NO_2 (a molecule with harmful effects on health and on environment) is, in fact, a common intermediate of NO abatement reaction. We also report in Fig. 7 (red lines) the total amount of nitrogen oxides in gas phase ($NO + NO_2 = NO_x$), a parameter that better represents the efficiency of the photocatalyst. Data in Fig. 7 clearly indicate that the material, in both irradiation conditions, shows the same total NOx abatement, with a similar kinetic. NO is nearly eliminated after 100 min while NO_2, generated in the initial steps of the test, reach a maximum in about 30 min and then slowly declines.

Finally, even though the material can absorb light over a wide range of the visible spectrum, no significant difference can be observed moving from the illumination with a monochromatic blue LED to a polychromatic white LED. This indicates that the blue light, the more efficient one in exciting intra band gap states due to nitrogen doping (Fig. 4), is crucial to activate the material and to its photocatalytic action.

3.4.2. *Photocatalytic activity under visible light in liquid phase*

Phenol was adopted as model pollutant since its degradation pathways have been extensively studied and it can be used to get insight into the photocatalytic activity of a given oxide [52]. The results of the photodegradation of phenol in solution are reported in Fig. 8 and Table 2. The figure also reports the concentrations (mg/L) of the main by-products of the photodegradation reaction, namely hydroquinone (HQ), p-benzoquinone (BQ) and catechol (CA). The total phenol abatement after 60 min of irradiation is 46.7% corresponding to an overall amount of 7 mg/L measured after the onset of the absorption-desorption equilibrium in dark. Comparing this concentration with those, much lower, of the by-products at 60 min, it is possible to infer that the majority of the phenol has gone beyond the first steps of degradation.

3.5. *Discussion*

3.5.1. *Origin of the visible light sensitization*

The spectroscopic characterization clearly shows that the C/N-TiO_2 material is able to absorb visible light and that this radiation induces the promotion of electrons to the conduction band. Such sensitization is, first of all, related to the presence of nitrogen and of the related intra-band gap states [33].

As shown by Eq. (1) it is mainly from the diamagnetic intra-bandgap NO^{3-} centres that electrons are photoexcited causing an increase of the amount of $NO^{2-\bullet}$ ones. This peculiar mechanism, clearly different from that acting in pristine TiO_2 under UV, explains the lack of holes detected by spin trapping. A hole formed by photoexcitation of the N doping centre (Eq. 1) is and remains localised on this centre (a highly localized intra-band-gap state) intrinsically lacking the capability to move in the crystal bulk that is typical of the holes generated in the valence band [53,54]. By the way photoformed holes are instead easily observed in our material when irradiation is performed using UV light with direct VB → CB excitation, bypassing the N intraband gap states (data not reported).

It has now to be considered that the reported characterization of the solid clearly indicates the presence of carbonaceous species deriving from the synthetic procedure. Incidentally, the carbon modification is an alternative way to sensitize TiO_2 to visible light [55]. For instance, in the case of the VLA material KRONOClean7000 (also based on modified titanium dioxide) the activation with visible light is attributed to the presence at the surface of carbon containing species, which act as antenna centres for the absorption of visible light, affecting also the lifetime of the photoinduced charge carriers [56].

In the present case we have shown that the presence of carbonaceous species causes an extension of the optical absorption from the blue region (mainly due to nitrogen centres) to higher wavelengths (Fig. 1 and Fig. S.I.2) and that irradiation using these wavelengths also causes photoreduction of oxygen (Eq. 3) though at a minor extent. This represents a first indication of the role of carbonaceous species i.e., of their photoactivity under visible frequencies as also confirmed by the intensity variations of the EPR signal of the carbon centred radical (Fig. 4) better appreciated comparing computer simulations of the spectra in dark and under irradiation (see Table S.I.1).

Despite the nature of the carbon photoactive species is still unclear, their behaviour is analogous to that of N containing species as they are excited by visible photons with promotion of electrons in the conduction band (capable to react with oxygen) and formation of additional amounts of $C^{\bullet}$ species, similarly to what proposed by E.A. Kostantinova et al. [57] In conclusion the VLA species in the solid capable to transfer electrons under irradiation are of two distinct types with the main role appointed to N bulk centre and a minor but non negligible role of surface carbonaceous species.

3.5.2. *Reactive oxygen species generated via visible light excitation*

Reactive Oxygen Species (ROS) play a crucial role in photocatalytic processes. Both solid state EPR (Fig. 4) and spin trapping experiments in solution (Fig. 5) confirm the formation of ROS under visible light irradiation only the O_2 derived species were observed. The formation of superoxide species observed both at the gas-solid and the liquid-solid interfaces ($O_2^{-\bullet}$, Eqs. 1–3) has been described in the previous Section (3.5.1). As previously discussed, no role of photogenerated holes was evidenced by our experiments (Fig. 6). The oxidizing action of the system relies therefore on the presence of superoxide ($O_2^{-\bullet}$) and singlet oxygen ($^1O_2$) species both remarkably generated by the action of visible light. As far as the singlet oxygen generation is concerned, it is worth to mention that this ROS is often observed when carbon containing species (carbon dots, dyes, graphene-like structures) are present in a photocatalytic system [58,59]. In general, the formation mechanism of this particularly reactive species involves energy or charge transfer from photogenerated triplet states or electron-hole pairs[60].

The same mechanism also operates in the present case considering that an abundant fraction of organic material is present at the surface of

Table 2
Phenol degraded (% and mg/L) and main intermediates concentration at 60 min of irradiation during the photocatalytic test.

	Phenol degr. %	Phenol degr. mg/L	HQ mg/L	BQ mg/L	CA mg/L
$\lambda > 420$	46.7	7.13	0.27	0.75	0.03

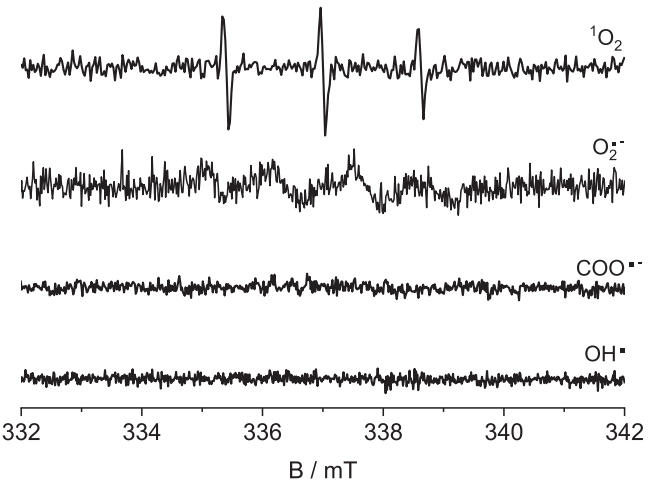

Fig. 5. EPR spectra resulting from spin trapping experiments. From the top: 4-OXO-TEMPO adduct after 30 min of irradiation with blue light; DMPO-O_2^- adduct recorded in acetonitrile solution after 10 min of irradiation with blue light. The other two adducts, DMPO-CO_2^- and DMPO-OH, were not detected.

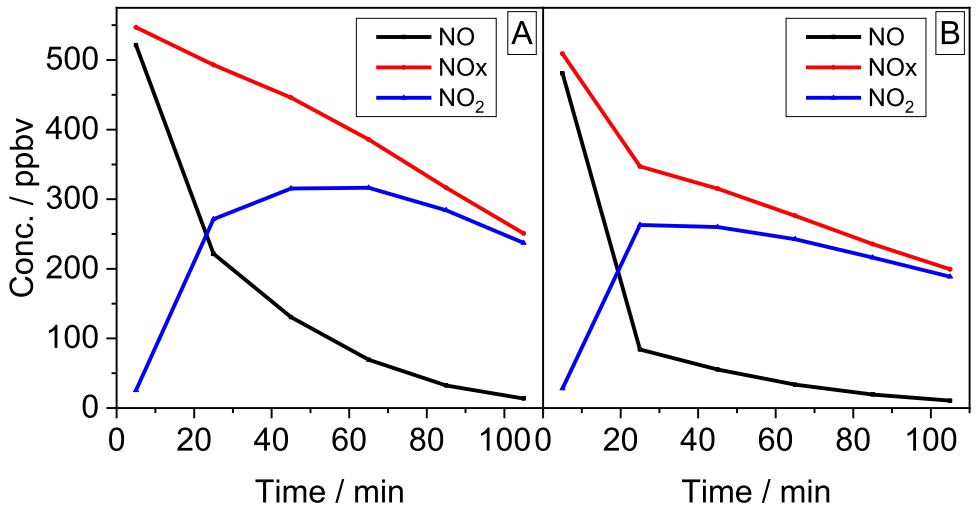

Fig. 6. Photocatalytic tests of NO (black curve), NO_2 (blue) and NO+NO_2 = NOx (red) degradation using two different LED lights. Panel A: NOx degradation under 3000 K LED (white LED). Panel B: NOx degradation under blue LED.

the solid, as indicated by thermogravimetric and spectroscopic data and depicted by Schemes 1 and 2. It is worth to mention also that singlet oxygen is active in the abatement of organic pollutants [61], but in this specific case its presence is probably detrimental for the full oxidation of NO. In fact, by removing the carbonaceous moieties from the surface using the procedure proposed by P. Zabek et al. [62], two important effects can be observed (see S.I. also) namely a dramatic reduction in $^1O_2$ generation capability (Fig. S.I. 9) and an increment of NO abatement capability. Fig. 8 reports the results of the test of NOx abatement using the sample treated with NaOH solution (0.5 M) overnight at 353 K in order to remove the organic fraction. After this treatment, the system was recovered by centrifugation, washed with deionized water (until neutral pH) and dried at 323 K. As clearly shown by Fig. 8 the treated sample presents a higher activity than that of the non-treated one (Fig. 7).

These evidences prove the role of the carbonaceous species in the formation of singlet oxygen, and more important, the detrimental effect of the $^1O_2$ species for the efficient NOx abatement in gas phase.

3.5.3. *Reaction mechanisms for C/N-TiO₂ under visible illumination*

In order to rationalize the mechanism acting in the two types of photocatalytic tests (gas and liquid phase respectively), the analysis starts from the phenomena occurring at the solid-liquid interface.

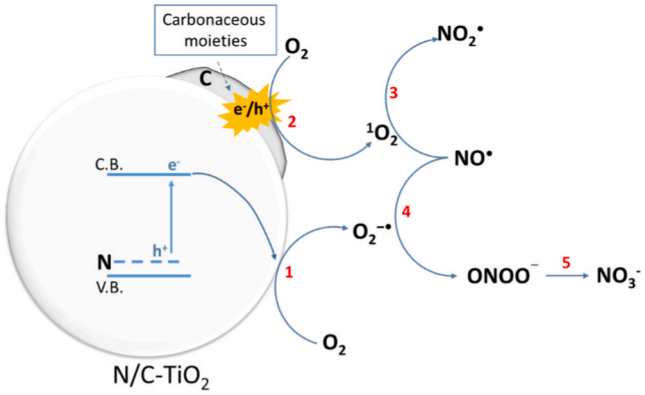

Scheme 2. Proposed mechanism acting in the NOx degradation in gas phase under irradiation with visible light. 1) Electron transfer from the conduction band to molecular oxygen at the surface of the system to form superoxide. 2) Energy transfer from excitons to oxygen molecules in order to form singlet oxygen. 3) Reaction between NO and singlet oxygen to form NO_2. 4) Reaction between NO and superoxide to form the $ONOO^-$ species. 5) Isomerization of $ONOO^-$ to NO_3^-.

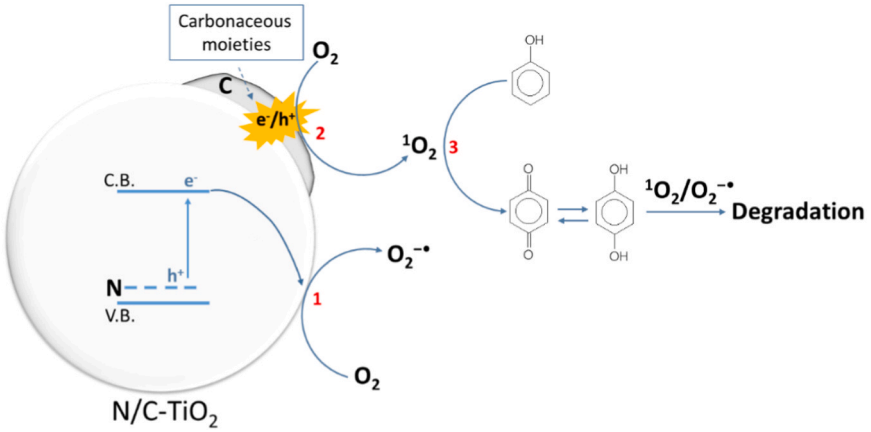

Scheme 1. Proposed mechanism acting in the phenol degradation in solution under irradiation with visible light. 1) Electron transfer from the conduction band to molecular oxygen at the surface of the system to form superoxide. 2) Energy transfer from excitons to oxygen molecules in order to form singlet oxygen. 3) Reaction between phenol and singlet oxygen to form benzoquinone, in equilibrium with hydroquinone. The degradation then continues thanks to both singlet oxygen and superoxide.

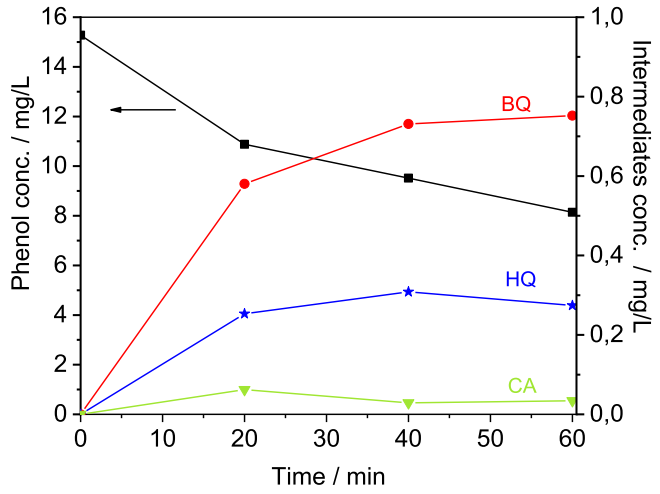

Fig. 7. Photocatalytic abatement of phenol in solution (black curve) under $\lambda > 420$ irradiation. Concentration in mg/L of the main intermediates produced during the degradation (BQ = benzoquinone, red; HQ= hydroquinone, blue; CA = catechol, green) are reported on the y axis on the right.

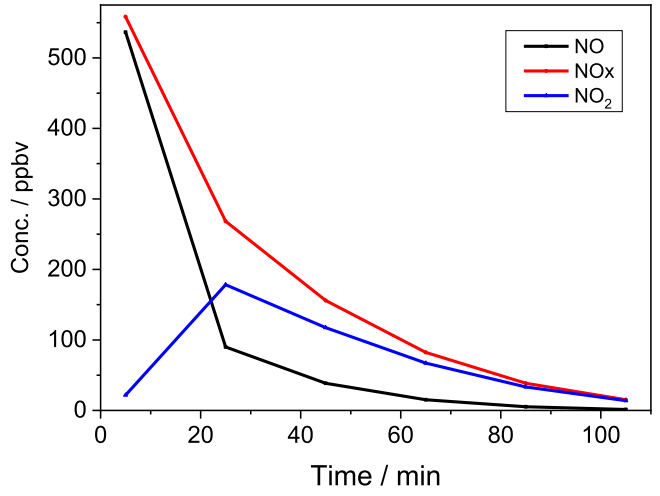

Fig. 8. NO abatement activity upon blue LED illumination in the case of the sample subjected to the surface treatment with NaOH.

Although $OH^{\bullet}$ radicals are usually the predominant active species in photocatalytic processes performed in aqueous solution, in the present case these species were not detected and the photocatalytic action only relies on dioxygen species ($^1O_2$ and $O_2^{-\bullet}$). In particular, singlet oxygen seems to lead the photocatalysis in liquid phase. This hypothesis is corroborated by data available in the literature. D. Zhang et al., for instance, show that in anhydrous solution, where $OH^{\bullet}$ radical cannot be formed, the singlet oxygen ($^1O_2$) is the predominant species responsible for the phenol degradation [63]. Furthermore, C. Li and M. Z. Hoffman have shown that singlet oxygen is able to oxidize the phenol to 1,4-benzoquinone (BQ). This, by the way, explains the fact that in our tests BQ is the most abundant species among the detected intermediates [64].

On the basis of these considerations the following scheme (Scheme 1) can be drawn to describe the photodegradation mechanism of phenol in solution.

Photogenerated electrons react with O_2 to form $O_2^{-\bullet}$, while holes remain localised on the N intra band gap states (Scheme 1, step 1). At the same time, irradiation of carbonaceous moieties located at the surface leads to the formation of electron/hole pairs (excitons). The energy coming from their recombination is transferred to $^3O_2$ forming singlet oxygen $^1O_2$ (Scheme 1, step 2). The $^1O_2$ species oxidize phenol to the first intermediate, benzoquinone. At this point, both singlet oxygen and superoxide contribute to the degradation pathway (Scheme 1, step 3).

Concerning the photocatalytic process involved in the NOx degradation in gas phase, the first part of the test is dominated by the oxidation of NO to NO_2 probably due to the presence of singlet oxygen in agreement with the following process.

$$2NO + {}^1O_2 \rightarrow 2NO_2 \quad (6)$$

Even though the presence this oxygen species has been detected in our experiments performed in aqueous medium its presence, since it is strictly related to the surface carbonaceous phase, is extremely likely also in gas phase reactions as reported in various investigations [65,66]. The material characterization also indicates that the other ROS species generated under visible light is the superoxide. This suggests that the complete oxidation of NO occurs at the expense of this species as reported for other photocatalysts [67]. For instance, it is well known that in some biological systems the interaction of NO with superoxide can give rise to peroxynitrite ($ONOO^-$), a well-known oxidant species [68] whose isomerization to NO_3^- is reported both in liquid and gas phase [69–71]. The same intermediate is invoked also in the case of chemical catalysts where $^1O_2$ is reported to be strictly related to the formation of NO_2 whereas the superoxide species drives the NO full oxidation via the peroxynitrite intermediate [72,73]. The whole process occurring at the surface of the photocatalyst in the case on NO abatement in gas phase can be thus roughly summarized by means of the processes described in Scheme 2.

Superoxide ions $O_2^{-\bullet}$ and singlet oxygen molecules are formed under illumination as described above in the case of phenol degradation. The $^1O_2$ species oxidize NO to NO_2 (Eq. 6, step 3). Superoxide $O_2^{-\bullet}$ ions react with NO generating the $ONOO^-$ species (step 4) which, in turn, give rise by isomerisation to the to fully oxidized NO_3^- ions (step 5).

The efficiency of the photocatalyst therefore depends on the interplay between steps 3 and 4. A minor role of step 3 (singlet oxygen) limits the formation of nitrogen dioxide allowing the reaction to proceed towards the full oxidation of nitric oxide. Therefore, the same singlet oxygen that has a central role in the degradation of phenol in liquid phase, has an opposite effect in gas phase. This is fully supported by the fact that removing the carbonaceous species leads to a system incapable of producing singlet oxygen (Fig. S.I. 9) but much more efficient in the NOx degradation (Figure 9). This result indicates that it is possible, in principle, to tune the properties of the photocatalyst simply modulating the amount of the surface carbonaceous phase. For instance, the presence of surface carbon containing spices can affect the electron transport efficiency to improve photo electrochemical applications.[74] The possibility of tuning the generated reactive oxygen species is in also a key aspect to design of efficient photocatalysts for a specific photoprocess., [75,76]. For instance, K. Zhang et al. studying the Tetracycline degradation reported that the joint use of light and temperature control can affect the singlet oxygen generation affecting in turn the final photoactivity.[77] Moreover, the singlet oxygen plays a pivotal role in the disinfection application or the selective organic synthesis [78,79]. In the present case, this allows to selectively orient the system towards a wanted application (e.g indoor air treatment vs. pollutant abatement in aqueous phase). Preliminary results of phenol degradation by N modified titania containing different amounts of surface carbonaceous phases confirm this view. Ad hoc systematic experiments on this peculiar property of the modified titania photocatalyst here described are currently in progress in our laboratories.

3.6. Conclusion

In this work a C/N-TiO_2 photocatalyst was characterized by monitoring both the physico-chemical properties and the photocatalytic activity in liquid and gas phase under visible light illumination. The EPR characterization indicates the presence of nitrogen containing centres,

associated to interstitial nitrogen, mainly responsible for the generation of superoxide ions $O_2^{-\bullet}$ under irradiation. A second reactive species (singlet oxygen, $^1O_2$) is formed owing to the action of a surface carbonaceous phase formed by decomposition of the modifier (ammonium citrate). Spin trapping experiments also showed the absence of reactive holes and related species ($OH^\bullet$ hydroxyl radicals, usually considered the most important active species in photocatalytic processes) since the photo excited electrons are generated from the mentioned intra band gap N centres so that the corresponding holes are strongly localized on the same centres. The material is nonetheless active in the oxidation of NO in gas phase and in phenol degradation in water solution. The singlet oxygen species has a crucial role in driving the photoactivity both in gas and liquid phase. In gas phase $^1O_2$ is detrimental for the photoefficiency, evaluated in terms of nitric oxide oxidation, whereas in liquid phase (phenol degradation) this species has a beneficial role. Summarizing we are facing a peculiar multitasking VLA material, whose properties can be modulated varying the content of surface carbonaceous species orienting thus the system toward different applications. The activity of this material under visible light (though lower than that of a "classic" titanium dioxide under UV) make it extremely interesting for applications where the use of UV radiation is not recommended such as in the indoor air purification.

CRediT authorship contribution statement

Alessia Zollo: Investigation, Writing – original draft, Formal analysis. **Stefano Livraghi:** Supervision, Writing – original draft. **Elio Giamello:** Supervision, Writing – review & editing. **Giovanni Baldi:** Supervision, Funding acquisition. **Andrea Cioni**: Methodology, Investigation. **Valentina Dami:** Formal analysis, Investigation. **Giada Lorenzi:** Investigation. **Stefano Agnoli:** Methodology, Investigation, Formal analysis. **Mateusz Adam Baluk:** Investigation. **Anna Gołąbiewska:** Methodology, Investigation. **Adriana Zaleska-Medynska:** Supervision - review.

Declaration of Competing Interest

The authors declare that they have no known competing financial interests or personal relationships that could have appeared to influence the work reported in this paper.

Data Availability

Data will be made available on request.

Acknowledgements

This research has received funding from the Project CH4.0 under the MUR program "Dipartimenti di Eccellenza 2023–2027" (CUP: D13C22003520001). This paper is part of a project that has received funding from the Compagnia di San Paolo, Torino, under the project SusNANOCatch "Sustainable strategies to reduce the presence in the environment of nanoparticles deriving from depollution processes"; from the European Union's Horizon 2020 research and innovation program under Marie Skłodowska-Curie grant agreement no. 101007578″ (SusWater).

Appendix A. Supporting information

Supplementary data associated with this article can be found in the online version at doi:10.1016/j.jece.2023.111523.

References

[1] T. Hisatomi, J. Kubota, K. Domen, Recent advances in semiconductors for photocatalytic and photoelectrochemical water splitting, Chem. Soc. Rev. 43 (2014) 7520–7535.
[2] D.F. Ollis, E. Pelizzetti, N. Serpone, Destruction of water contaminants, Environ. Sci. Technol. 25 (1991) 1522–1529.
[3] K. Hashimoto, H. Irie, A. Fujishima, TiO_2 Photocatalysis: a historical overview and future prospects, Jpn. J. Appl. Phys. 44 (2005) 8269–8285.
[4] M.R. Hoffman, S.T. Martin, W. Choi, D.W. Bahnemann, Environmental applications of semiconductor photocatalysis, Chem. Rev. 95 (1995) 69–96.
[5] T. Matsunaga, R. Tomoda, T. Nakajima, H. Wake, Photoelectrochemical sterilization of microbial cells by semiconductor powders, FEMS Microbiol. Lett. 29 (1985) 211–214.
[6] S. Smolinski, D.M. Blake, Z. Huang, E.J. Wolfrum, W. Jacoby, Bactericidal activity of photocatalytic TiO_2 reaction: toward an understanding of its killing mechanism, Appl. Environ. Microbiol. 65 (1999) 4094–4098.
[7] H.A. Foster, I.B. Ditta, S. Varghese, A. Steele, Photocatalytic disinfection using titanium dioxide: spectrum and mechanism of antimicrobial activity, Appl. Microbiol. Biotechnol. 90 (2011) 1847–1868. DOI 10.1007/s00253-011-3213-7.
[8] A. Fujishima, K. Honda, Electrochemical photolysis of water at a semiconductor electrode, Nat. Biotechnol. 238 (1972) 37–38.
[9] A. Kudo, Y. Miseki, Heterogeneous photocatalyst materials for water splitting, Chem. Soc. Rev. 38 (2009) 253–278.
[10] Q. Wang, K. Domen, Particulate photocatalysts for light-driven water splitting: mechanisms, challenges, and design strategies, Chem. Rev. 120 (2020), 919–985.
[11] X. Wang, K. Maeda, A. Thomas, K. Takanabe, G. Xin, J.M. Carlsson, K. Domen, M. Antonietti, A metal-free polymeric photocatalyst for hydrogen production from water under visible light, Nat. Mater. 8 (2009) 76–80.
[12] P. Wang, B. Huang, Y. Dai, M.-H. Whangbo, Plasmonic photocatalysts: harvesting visible light with noble metal nanoparticles, Phys. Chem. Chem. Phys. 14 (2012) 9813–9825.
[13] P. Zhou, J. Yu, M. Jaroniec, ll-solid-state Z-scheme photocatalytic systems, Advan, Materials 26 (2014) 4920–4935.
[14] S. Sato, R. Nakamura, S. Abe, Visible-light sensitization of TiO_2 photocatalysts by wet-method N doping, Appl. Catal. A 284 (2005) 131–137.
[15] R. Asahi, T. Morikawa, T. Ohwaki, K. Aoki, Y. Taga, Visible-light photocatalysis in nitrogen-doped titanium oxides, Science 293 (2001) 269–271.
[16] R. Asahi, T. Morikawa, H. Irie, T. Ohwaki, Nitrogen-doped titanium dioxide as visible-light-sensitive photocatalyst: designs, developments, and prospects, Chem. Rev. 114 (2014) 9824–9852.
[17] J.M. Samet, M.C. Marbury, J.D. Spengler, Health effects and sources of indoor air pollution. Part I, Am. Rev. Respir. Dis. 136 (1987) 1486–1508.
[18] A.P. Jones, Indoor air quality and health, Atmos. Environ. 33 (1999) 4535–4564.
[19] S.M. Verbruggen, TiO_2 photocatalysis for the degradation of pollutants in gas phase: From morphological design to plasmonic enhancement, J. Photochem. Photobiol. C: Photochem. Rev. 24 (2015) 64–82.
[20] A. Luengas, A. Barona, C. Hort, G. Gallastegui, V. Platel, A. Elias, A review of indoor air treatment technologies, Rev. Environ. Sci. Biotechnol. 14 (2015) 499–522.
[21] X. Wang, T.-T. Lim, Solvothermal synthesis of C–N codoped TiO_2 and photocatalytic evaluation for bisphenol A degradation using a visible-light irradiated LED photoreactor, Appl. Cat. B: Environ. 100 (2010) 355–364.
[22] V. Trevisan, A. Olivo, F. Pinna, M. Signoretto, F. Vindigni, G. Cerrato, C.L. Bianchi, C-N/TiO_2 photocatalysts: Effect of co-doping on the catalytic performance under visible light, Appl. Cat. B: Environ. 160 161 (2014) 152–160.
[23] S. Komatsuda, Y. Asakura, J.J.M. Vequizo, A. Yamakata, Shu Yin, Enhanced photocatalytic NOx decomposition of visible-light responsive F-TiO_2/(N,C)-TiO_2 by charge transfer between F-TiO_2 and (N,C)-TiO_2 through their doping levels, Appl. Cat. B: Environ. 238 (2018) 358–364.
[24] B. Malini, G. Allen Gnana Raj, C,N and S-doped TiO_2-characterization and photocatalytic performance for rose bengal dye degradation under day light, J. Environ. Chem. Eng. 6 (2018) 5763–5770.
[25] A.J. Moreira, B.R.M. dos Santos, J.A. Dias, P.T. Rabello, D. Coelho, L.H. Mascar, G. P.G. Freschi, Y.G. Gobato, H.V.A. Galeti, V.R. Mastelaro, E.C. Pereira, Photoactivity of boron-or nitrogen-modified TiO_2 for organic pollutants degradation: Unveiling the photocatalytic mechanisms and by-products, J. Environ. Chem. Eng. 11 (2023), 109207.
[26] C. Di Valentin, G. Pacchioni, A. Selloni, S. Livraghi, E. Giamello, Characterization of paramagnetic species in N-doped TiO_2 powders by EPR spectroscopy and DFT calculations, J. Phys. Chem. B 109 (2005) 11414–11419.
[27] S. Livraghi, M.C. Paganini, E. Giamello, A. Selloni, C.D. Valentin, G. Pacchioni, Origin of photoactivity of nitrogen-doped titanium dioxide under visible light, J. Am. Chem. Soc. 128 (2006) 15666–15671.
[28] G. Barolo, S. Livraghi, M. Chiesa, M.C. Paganini, E. Giamello, Mechanism of the Photoactivity under visible light of N-doped titanium dioxide. Charge carriers migration in irradiated N-TiO_2 Investigated by Electron Paramagnetic Resonance, J. Phys. Chem. C. 116 (2012) 20887–20894.
[29] C. Di Valentin, G. Pacchioni, A. Selloni, Theory of Carbon Doping of Titanium Dioxide, Chem. Mater. 17 (2005) 6656–6665.
[30] H. Zhang, X. Lv, Y. Li, Y. Wang, J. Li, P25-Graphene Composite as a High Performance Photocatalyst, ACS Nano 4 (1) (2010) 380–386.
[31] R. Leary, A. Westwood, Carbonaceous nanomaterials for the enhancement of TiO_2 Photocatalysis, CARBON 49 (2011) 741–772.

[32] C. Han, Y. Wang, Y. Lei, B. Wang, N. Wu, Q. Shi, Q. Li, In situ synthesis of graphitic-C_3N_4 nanosheet hybridized N-doped TiO_2 nanofibers for efficient photocatalytic H_2 production and degradation, Nano Res 8 (2015) 1199.
[33] D. Mitoraj, H. Kisch, The nature of nitrogen-modified titanium dioxide photocatalysts active in visible light, Angew. Chem. Int. Ed. 47 (2008) 9975–9978.
[34] N.G. Moustakas, A.G. Kontos, V. Likodimos, F. Katsaros, N. Boukos, D. Tsoutsou, A. Dimoulas, G.E. Romanos, D.D. Dionysiou, P. Falaras, Inorganic–organic core–shell titania nanoparticles for efficient visible light activated photocatalysis, Appl. Cat. B: Environ. 130–131 (2013) 14–24.
[35] W. Jiang, M. Zhang, J. Wang, Y. Liu, Y. Zhu, Dramatic visible activity in phenol degradation of TCNQ@TiO_2 photocatalyst with core-shell structure, Appl. Cat. B: Environ. 160–161 (2014) 44–50.
[36] L. Chang, N. Ahmad, G. Zeng, A. Ray, Y. Zhang, N, S co-doped carbon quantum dots/TiO_2 composite for visible-light-driven photocatalytic reduction of Cr (VI) J, Environ. Chem. Eng. 10 (2022), 108742.
[37] Z.W. Heng, W.C. Chong, Y.L. Pang, C.H. Koo, An overview of the recent advances of carbon quantum dots/metal oxides in the application of heterogeneous photocatalysis in photodegradation of pollutants towards visible-light and solar energy exploitation, J. Environ. Chem. Eng. 9 (2021), 105199.
[38] S. Livraghi, I. Corazzari, M.C. Paganini, G. Ceccone, E. Giamello, B. Fubinia, I. Fenoglio, Decreasing the oxidative potential of TiO_2 nanoparticles through modification of the surface with carbon: a new strategy for the production of safe UV filters, Chem. Commun. 46 (2010) 8478–8480.
[39] P. Mazierski, M. Nischk, M. Gołkowska, W. Lisowski, M. Gazdac, M.J. Winiarskic, T. Klimczuk, A. Zaleska-Medynskaa, Photocatalytic activity of nitrogen doped TiO_2 nanotubes prepared byanodic oxidation: The effect of applied voltage, anodization time and amount of nitrogen dopant, Appl. Cat. B: Environ. 196 (2016) 77–88.
[40] Y. Qiu, Z. Wang, A.C.E. Owens, I. Kulaots, Y. Chen, A.B. Kanec, R.H. Hurt, Antioxidant chemistry of graphene-based materials and its role in oxidation protection technology, Nanoscale 6 (2014) 11744–11755.
[41] A. Zollo, S. Livraghi, E. Giamello, A. Cioni, V. Dami, G. Lorenzi, G. Baldi, C-N co-doped titanium dioxide. Key aspects in the assessment of the air pollutants abatement capability, J. Environ. Chem. Eng. 11 (2023), 109451-109461.
[42] E. Paradisi, M. Lassinanti Gualtieri, P. Veronesi, V. Dami, G. Lorenzi, A. Cioni, G. Baldi, C. Leonelli, Crucible effect on phase transition temperature during microwave calcination of a N-Doped TiO_2 precursor: implications for the preparation of TiO_2 nanophotocatalysts, ACS Appl. Nano Mater. 6 (7) (2023) 5448–5459.
[43] M. Chiesa, S. Livraghi, M.C. Paganini, Enrico Salvadori, E. Giamello, Nitrogen-doped semiconducting oxides. Implications on photochemical, photocatalytic and electronic properties derived from EPR spectroscopy, Chem. Sci. 11 (2020) 6623–6641.
[44] R. Ashai, T. Morikawa, Nitrogen complex species and its chemical nature in TiO_2 for visible-light sensitized photocatalysis, Chem. Phys. 339 (2007) 57–63.
[45] S.Y. Lim, W. Shen, Z. Gao, Carbon quantum dots and their applications, Chem. Soc. Rev. 44 (2015) 362–381.
[46] Z. Yang, M. Xu, Y. Liu, F. He, F. Gao, Y. Su, H. Wei, Y. Zhang, Nitrogen-doped, carbon-rich, highly photoluminescent carbon dots from ammonium citrate, Nanoscale 6 (2014) 1890–1895.
[47] N. Xu, H. Huang, H. Ouyang, H. Wang, Preparation of the heterojunction catalyst N-doping carbon quantum dots/P25 and its visible light photocatalytic activity, Sci. Rep. 9 (2019) 9971.
[48] M. Chiesa, E. Giamello, S. Livraghi, M.C. Paganini, V. Polliotto, E. Salvadori, Electron magnetic resonance in heterogeneous photocatalysis research, J. Condens. Matter Phys. 31 (2019), 444001.
[49] V. Polliotto, S. Livraghi, E. Giamello, Electron magnetic resonance as a tool to monitor charge separation and reactivity in photocatalytic materials, Res. Chem. Intermed. 44 (2018) 3905–3921.
[50] F. Parrino, S. Livraghi, E. Giamello, R. Ceccato, L. Palmisano, Role of hydroxyl, superoxide, and nitrate radicals on the fate of bromide ions in photocatalytic TiO_2 suspensions, ACS Catal. 10 (2020) 7922–7931.
[51] M. Anpo, G. Costentin, E. Giamello, H. Lauron-Pernot, Z. Sojka, Characterisation and reactivity of oxygen species at the surface of metal oxides, J. Catal. 393 (2021) 259–280.
[52] D. Vionea, C. Minero, V. Maurino, M.E. Carlotti, T. Picatonotto, E. Pelizzetti, Degradation of phenol and benzoic acid in the presence of a TiO_2-based heterogeneous photocatalyst, Appl. Cat. B: Environ. 58 (2005) 79–88.
[53] M. Mrowetz, W. Balcerski, A.J. Colussi, M.R. Hoffmann, Oxidative Power of Nitrogen-Doped TiO_2 Photocatalysts under Visible Illumination, J. Phys. Chem. B 108 (2004) 17269–17273.
[54] T. Fotiou, T.M. Triantis, T. Kaloudis, K.E. O'Shea, D.D. Dionysiou, A. Hiskia, Assessment of the roles of reactive oxygen species in the UV and visible light photocatalytic degradation of cyanotoxins and water taste and odor compounds using C-TiO_2, Water Res. 90 (2016) 52–61.
[55] C. Di Valentin, G. Pacchioni, A. Selloni, Theory of carbon doping of titanium dioxide, Chem. Mater. 17 (2005) 6656–6665.
[56] D.M. Tobaldi, M.P. Seabra, G. Otero-Irurueta, Y.R. de Miguel, R.J. Ball, M.K. Singh, R.C. Pullara, J.A. Labrinch, Quantitative XRD characterisation and gas-phase photocatalytic activity testing for visible-light (indoor applications) of KRONOClean 7000®, RSC Adv. 5 (2015), 102911.
[57] E.A. Kostantinova, A.I. Kokotin, S. Sakthivel, H. Kisch, K. Lips. Carbon-doped titanium dioxide: visible light photocatalysis and EPR investigation, CHIMIA 61 (2007) 810–814.
[58] Y.-H. Chen, B.-K. Wang, W.-C. Hou, Graphitic carbon nitride embedded with graphene materials towards photocatalysis of bisphenol A: The role of graphene and mediation of superoxide and singlet oxygen, Chemosphere 278 (2021), 130334.
[59] M. Mikrut, O. Mazuryk, W. Macyk, R. van Eldik, G. Stochel, Generation and photogeneration of hydroxyl radicals and singlet oxygen by particulate matter and its inorganic components, J. Environ. Chem. Eng. 9 (2021), 106478.
[60] M. Tamtaji, A. Tyagi, C.Y. You, P.R. Galligan, H. Liu, Z. Liu, Singlet, Oxygen Photosensitization Using Graphene-Based Structures and Immobilized Dyes: A Review. ACS Appl. Nano Mater. 4 (2021) 7563–7586.
[61] P. Górska, A. Zaleska, E. Kowalska, T. Klimczuk, J.W. Sobczak, E. Skwarek, W. Janusz, J. Hupka, TiO_2 photoactivity in vis and UV light: The influence of calcination temperature and surface properties, Appl. Catal. B: Environ. 84 (2008) 440–447.
[62] P. Zabek, J. Eberl, H. Kisch, On the origin of visible light activity in carbon-modified titania, Photochem. Photobiol. Sci. 8 (2009) 264–269.
[63] D. Zhang, R. Qiu, L. Song, B. Eric, Y. Mo, X. Huang, Role of oxygen active species in the photocatalytic degradation of phenol using polymer sensitized TiO_2 under visible light irradiation, J. Hazard. Mater. 163 (2009) 843–847.
[64] C. Li, M.Z. Hoffman, Oxidation of phenol by singlet oxygen photosensitized by the tris(2,2'-bipyridine) ruthenium(II) ion, J. Phys. Chem. A 104 (2000) 5998–6002.
[65] M. Oluwatoyin Sunday, H. Sakugawa, A simple, inexpensive method for gas-phase singlet oxygen generation from sensitizer-impregnated filters: Potential application to bacteria/virus inactivation and pollutant degradation, Sci. Total Environ. 746 (2020), 141186.
[66] K. Wang, S. Song, S. Jung, J. Hwang, M. Kim, J. Kim, J. Sung, J. Lee, Y. Kim, Lifetime and diffusion distance of singlet oxygen in air under everyday atmospheric conditions, Phys. Chem. Chem. Phys. 22 (2020) 21664.
[67] Q. Zhang, Y. Shi, X. Shi, T. Huang, S. Lee, Y. Huang, J.-j Cao, Constructing Pd/ferroelectric $Bi_4Ti_3O_{12}$ nanoflake interfaces for O_2 activation and boosting NO photo-oxidation, Appl. Cat. B: Environ. 302 (2022), 120876.
[68] R. Radi, Oxygen radicals, nitric oxide, and peroxynitrite: Redox pathways in molecular medicine, PNAS 115 (2018) 5839–5848.
[69] B.D. Bean, A.K. Mollner, S.A. Nizkorodov, G. Nair, M. Okumura, S.P. Sander, K. A. Peterson, J.S. Francisco, Cavity ringdown spectroscopy of cis-cis HOONO and the HOONO/$HONO_2$ branching ratio in the reaction OH + NO_2 + M, J. Phys. Chem. A 107 (2003) 6974–6985.
[70] Y. Zhao, K.N. Houk, L.P. Olson, Mechanisms of peroxynitrous acid and methyl peroxynitrite, ROONO (R = H, Me), rearrangements: A conformation-dependent homolytic dissociation, J. Phys. Chem. A 108 (2004) 5864–5871.
[71] S.K. Sharma, A.W. Schaefer, H. Lim, H. Matsumura, P. Moënne-Loccoz, B. Hedman, K.O. Hodgson, E.I. Solomon, K.D. Karlin, A six-coordinate peroxynitrite low-spin iron(III) porphyrinate complex—The product of the reaction of nitrogen monoxide (·NO(g)) with a ferric-superoxide species, J. Am. Chem. Soc. 139 (2017) 17421–17430.
[72] H. Li, H. Shang, X. Cao, Z. Yang, Z. Ai, L. Zhang, Oxygen vacancies mediated complete visible Light NO oxidation via side-on bridging superoxide radicals, Environ. Sci. Technol. 52 (2018) 8659–8665.
[73] Y. Shi, Z. Yang, L. Shi, H. Li, X. Liu, X. Zhang, J. Cheng, C. Liang, S. Cao, F. Guo, X. Liu, Z. Ai, L. Zhang, Surface boronizing can weaken the excitonic effects of BiOBr nanosheets for efficient O_2 activation and selective NO oxidation under visible light irradiation, Environ. Sci. Technol. 56 (2022) 14478–14486.
[74] Y. Wang, Y. Zhao, P. Zhu, X. Wu, A. Koshayeva, L. Ding, G. Wei, Y. Su, A promising one-step carbothermal reduction nitridation strategy for enhancing photoelectrochemical performance of TiO_2 nanowire array-based catalysts with stable nitrogen doping and desired core-double shell structure, Appl. Surf. Sci. 639 (2023), 158261.
[75] R. Zhou, D. Zhang, P. Wang, Y. Huang, Regulation of excitons dissociation in AgI/Bi_3O_4Br for advanced reactive oxygen species generation towards photodegradation, Appl. Cat. B: Environ. 285 (2021), 119820.
[76] H. Yan, Y. Deng, M. Shen, Y.-X. Ye, F. Zhu, X. Yang, G. Ouyang, Regulation the reactive oxygen species on conjugated polymers for highly efficient photocatalysis, Appl. Cat. B: Environ. 314 (2022), 121488.
[77] K. Zhang, Y. Wei, H. Cao, Y. Xin, C. Wang, Modulation of reactive species in peroxymonosulfate activation by photothermal effect: A case of MOF-derived $ZnFe_2O_4$/C, Sep. Purif. Technol. 306 (2023), 122732.
[78] M.C. DeRosa, R.J. Crutchley, Photosensitized singlet oxygen and its applications, Coord. Chem. Rev. 233–234 (2002) 351–371.
[79] R. Ciriminna, F. Parrino, C. De Pasquale, L. Palmisano, M. Pagliaro, Photocatalytic partial oxidation of limonene to 1,2 limonene oxide, Chem. Commun. 54 (2018) 1008–1011.